Research Article

# Microwave heating and processing of solid metals using electromagnetic resonators

Jing Zhou[1], Yingguang Li[1,*], Tao Yang [1], Wenzheng Xue[1], Xiaozhong Hao[1], James Gao[2]

[1]*National Key Laboratory of Science and Technology on Helicopter Transmission, Nanjing University of Aeronautics and Astronautics, Nanjing, 210016, China*

[2]*School of Engineering, University of Greenwich, Chatham Maritime, Kent ME4 4TB, UK*

*Corresponding author. Email: liyingguang@nuaa.edu.cn

**Abstract:** Heating plays a vital role in various manufacturing processes of metallic products. Microwave heating has many advantages over conventional conductive heating methods whilst it is currently limited to heating dielectric materials and powdered metals. This paper reports a new microwave heating method using electromagnetic resonators, which was, for the first time, proved effective for heating solid metals. This is a quite promising discovery, because as known, solid metals are essentially reflective of microwaves, and thus metallic objects are often prohibited in microwave ovens. The experiment results showed almost complete microwave absorption and excellent heating performance for a range of metal plates including both magnetic (e.g., iron, nickel and invar) and non-magnetic (e.g., tin and zinc). A patterned microwave heating process was also presented by adjusting electromagnetic resonators and microwave radiations. On this basis, a new multi-zone microwave processing paradigm was developed and demonstrated for welding metal plates. The research work may not only provide potential solutions for efficient heating and processing of complex shaped metal parts, but also enable a plethora of applications like localized heating and thermal display.

**Keywords:** Solid metals; Microwave heating; Welding; Electromagnetic resonators

## 1 Introduction

Heating is required in various manufacturing processes of metallic products such as forming [1],[2], heat treatments [3],[4] and welding [5],[6] , because the microstructure and properties of

metallic materials are closely associated with temperature [7]. For example, heating is often applied before metal forming (annealing), after metal forming (hardening or annealing) and sometimes during the metal forming process [8]. Heating may also be required for metallic products during service. For instance, Halford [10] developed a heated tooling system for increased control of moulded material properties. Therefore, it is crucial to develop effective and efficient heating technologies for metallic products.

Current metal heating methods are mainly based on heat transfer, light absorption, electric current and alternating magnetic fields. Furnaces are widely used to heat metallic parts (of large size and complex shape) through heat convection and radiation [10]. Contact heating methods through conduction were also developed, which could heat metal parts either uniformly or partially [11]. However, heating efficiency is low and environmental pollution is high using furnaces, while contact heating is usually limited to small parts. Light absorption is of great significance in the field of laser technologies which is able to heat components rapidly and locally. For example, Duflou et al. [12] developed a laser assisted incremental forming method allowing to differentiate material properties in time and space. Lee et al. [13] reported a similar local heating method by near-infrared rays used for the forming process of non-quenchable advanced high-strength steels. Selective heating methods offer the possibility to heat only the areas of the component where strongest deformations are required, and thus have outstanding advantages in improving the flexibility of metal forming processes [1]. However, the light absorption of the material is depended on its structure and composition which is generally low on smooth metal surfaces. As indicated by Biesuz et al. [14], metals reflect 40% - 95% of the radiation in the visible and near-ultraviolet, and 90%-99% in the infrared rays. Resistance heating methods based on electric current and induction heating based on alternating magnetic fields have prominent advantages in terms of high heating rate and energy efficiency. For instance, Mori et al. [15] proposed a hot stamping process using resistance heating to improve productivity. In this pioneering work, the heating process was so rapid (to 800°C in 2 seconds) that it can synchronize with the forming process. However, resistance heating is usually limited to regular shaped parts of constant cross-

sections, and the temperature distribution in the contacting area between the electrode and the part is not even [16]. Although induction heating does not have limitations on the shapes and cross-sections of parts [17], the design of inductors for complex shaped parts can be difficult (inductors have to be carefully fitted to various positions on the surfaces of complex parts). Its efficiency is also low for metals with low magnetic permeability.

By comparison, microwave heating has a high heating rate and energy efficiency [18]-[22], and has no limitation on part shapes, as energy is applied to the part (component) by an electromagnetic field [23],[24] [24]. For example, rapid energy-efficient heating of carbon fiber reinforced polymer composite laminates was realized by Zhou et al. [25], where an improvement of 36.3 times in heating efficiency and a reduction of 99.2% in energy consumption were achieved, compared with conventional autoclaves. Similarly, microwaves are considered to have great potential for efficient heating of large and complex shaped solid metals, and can be integrated into manufacturing processes such as forming, welding and heat treatment. However, solid metals are microwave reflective below certain critical temperatures (around half of the melting temperatures of respective solid metals) [26]. Therefore, microwave heating had been only effectively used for heating dielectric materials. Until 1999, microwave heating of powdered metals was reported by Roy et al. [27]. In 2018, the microwave absorption mechanism of metallic powders was analyzed by Zhang et al. [28]. To the best knowledge of the authors, microwave heating of solid metals has not been successfully realized, and metallic objects are still prohibited in microwave ovens.

This paper reports a new method that makes solid metals completely microwave absorptive below the critical temperatures using electromagnetic resonators (EMRs). Microwave heating of various solid metals, including magnetic metals (e.g., iron, nickel and invar) and non-magnetic metals (e.g., tin and zinc) were tested with excellent results. A patterned microwave heating process was realized, and a new multi-zone microwave processing paradigm was demonstrated for welding.

## 2 The proposed methodology

### 2.1 Problem definition and principles of the proposed idea

In principle, when a microwave electric field is applied to a solid metal, the large number of free electrons in the metal will redistribute immediately, forming an internal electric field with the same magnitude as the applied electric field but in the opposite direction. As a result, the microwave will be reflected. The movement of electrons is accompanied by energy conversion, just like resistance heating. Therefore, the authors established the hypothesis that the reason why solid metals cannot be heated by microwave is that the induced current is too low. If a high current on the solid metal can be generated, microwave heating of metals may be realized.

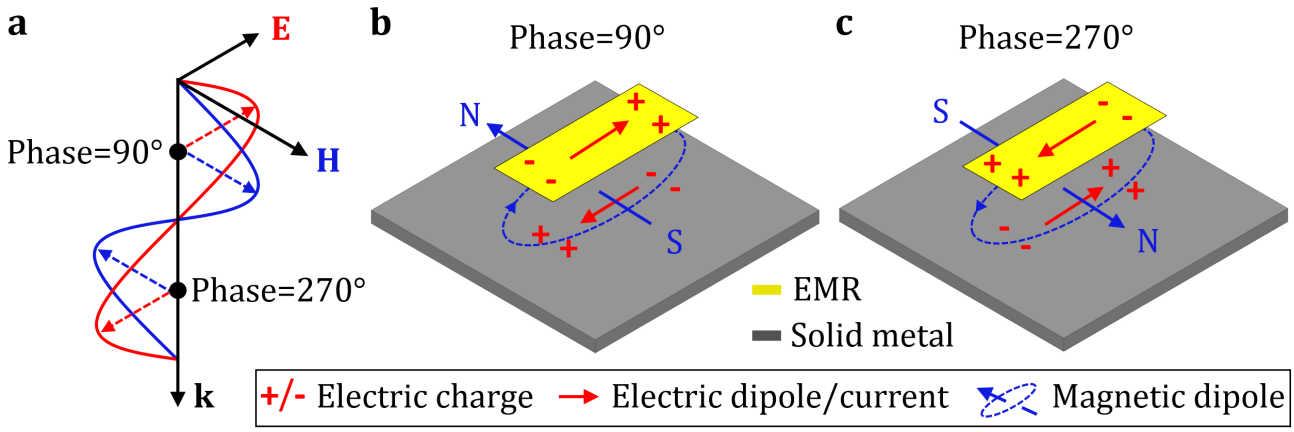


**Fig. 1.** The normally incident microwave signal (a) and the response of the EMRs and solid metal (b-c), where **E**, **H**, and **k** denote the direction of the electric field, magnetic field and wave propagation respectively.

In this study, the resonance principle [29] was adopted to amplify the current density on the cross-section of solid metals. Specifically, subwavelength metallic EMRs were introduced on solid metals with a small gap between them. Taking one normally incident microwave signal as an example. As shown in Fig. 1(a), a time-varying electric current is generated in the EMRs. At the same time, a reverse electric current will be induced in the adjacent solid metal as depicted in Fig. 1(b) and (c). In this way, electric dipoles are formed by the accumulated electric charge, and a magnetic dipole is formed by the antiparallel current pairs [30]. Note that both the electric and magnetic dipoles frequently change

directions, and they also interact with the electric and magnetic fields of the microwave. With appropriate design (e.g., with the aid of electromagnetic simulation) of the EMRs, both electric and magnetic resonance can be achieved. Thus, the pairing currents induced in the EMRs and the solid metal can be very high, resulting in a high heating effect on the solid metal. Note that high conductivity materials can be used for EMRs to reduce their energy consumption (e.g., copper, silver and graphene).

### 2.2 Design of electromagnetic resonators

Since microwaves are incident on the object being heated at various angles and the electric and magnetic fields also distribute in various directions accordingly, EMRs with symmetrical geometry can achieve better microwave absorption than irregular geometry. In this research , a copper ring was adopted which avoided intense current accumulation in the center (thus more uniform). As shown in Fig. 2, a dielectric spacer was used to support EMRs and maintain the gap between the EMRs and the solid metal. The combination of the EMRs, dielectric spacer and solid metal is termed the "Metal-Insulator-Metal (MIM) configuration". As shown in Fig. 2, $a$ is the dimension of the square-shaped constituent element; $r_1$ and $r_2$ are the outer and inner radius of the EMR; $h_1$, $h_2$, $h_3$ are the thickness of the EMR, dielectric spacer and solid metal, respectively.

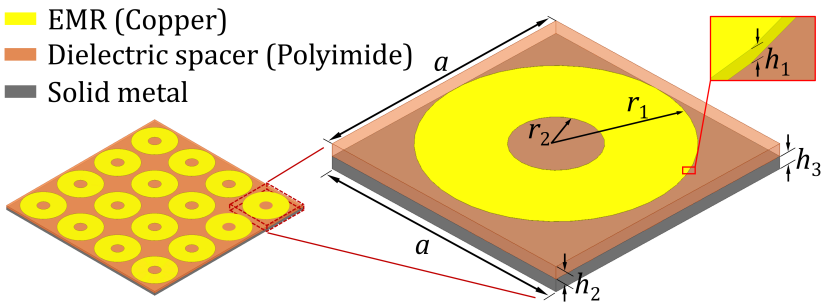


**Fig. 2.** The MIM configuration and its constituent elements.

In practice, $h_3$ does not influence microwave absorption of MIM configurations, because it is usually greater than the depth of the microwave penetration into metals (in microns). Thus, this method applies to solid metals of different thicknesses. $h_1$ is specified as 18 microns. One consideration is the flexibility of EMRs. The other is the availability and machinability of raw materials. $a$, $r_1$, $r_2$ and $h_2$

are closely related to the electric and magnetic resonance, and should be designed carefully. Frequency-dependent simulations have been carried out to predict the absorption of potential MIM configurations from which the value of these dimensions is determined to ensure an almost complete microwave absorption. The simulation model was constructed in the High-Frequency Structure Simulator, in which a microwave signal of 1 W (schematically illustrated by Fig. 3(a)) was irradiated on an infinite MIM configuration using master and slave boundaries [25].

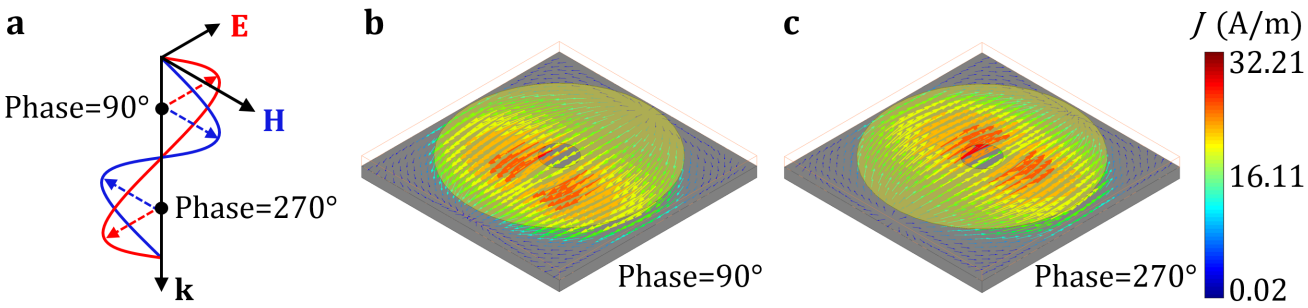


**Fig. 3.** (a) The normally incident microwave signal (1 W). (b-c) The simulated current distribution on the EMR-covered iron surface.

**Table 1**

Electromagnetic properties of adopted metals and the determined dimensions of corresponding MIM configurations.

| Materials | Tin | Zinc | Iron | Nickel | Invar |
|---|---|---|---|---|---|
| Conductivity ($10^6$ S/m) | 8.67 | 16.70 | 10.30 | 14.50 | 1.42 |
| Permeability (1) | 1 | 1 | 4000 | 600 | 1500 |
| $a$ (mm) | 39.00 | 36.50 | 39.00 | 39.00 | 33.00 |
| $r_1$ (mm) | 17.50 | 16.25 | 17.50 | 17.50 | 14.50 |
| $r_2$ (mm) | 4.50 | 6.00 | 3.00 | 4.25 | 7.75 |
| $h_2$ (mm) | 0.50 | 0.50 | 1.75 | 1.25 | 2.50 |

Without loss of generality, 5 metals (i.e., tin, zinc, iron, nickel and invar) were studied in this research, covering non-magnetic, magnetic, pure metal and alloy. The electromagnetic properties of

these materials and the determined dimensions of corresponding MIM configurations are summarized in Table 1. Taking iron as an example, Fig. 3(b) and (c) show the simulated distribution of the surface current *J* on the EMR-covered iron plate, which is consistent with the principles illustrated in Fig. 1(b) and (c). As shown, the peak value of the electric current in the area covered by the EMRs reached 32.21 A/m under the radiation of the microwave signal of 1 W. It is several orders of magnitude higher than that in the uncovered area (about 0.02 A/m), which demonstrated the effectiveness of the method. Moreover, a relatively uniform current distribution was achieved in the EMR-covered areas, which was mainly ascribed to the effect of the hole designed at the center of the EMR. It should be noted that the induced current oscillated at the same frequency as the incident microwave (2.45 GHz). As soon as the microwave was withdrawn, the current disappeared immediately. In addition, the induced current decreased quickly in the thickness direction, which was determined by the depth of penetration into metal materials. Fortunately, metal materials usually have excellent thermal conduction properties, which allows heat generated on the surface to be quickly transferred to the whole metal part.

## 3 Experiments

### 3.1 Sample prepration and fabrication

A copper-clad polyimide film was used to prepare the EMRs. The thickness of the copper and the polyimide layers was 18 μm and 0.25 mm, respectively. After the design of EMRs, copper-clad polyimide films were etched with the required periodic planar structure by a laser printed circuit board etcher (ProtoLaser U4, LPKF). Then, several polyimide films (without copper layers) were stacked up to form the dielectric spacer. The thickness of the polyimide film was also 0.25 mm. After that, the dielectric spacer with EMRs on its upper surface was put on the surface of a metal plate, and the whole configuration was packaged and closely attached by vacuuming. In this experiment, five metal plates were used, including tin, zinc, iron, nickel and invar. They were provided by Shenghang Metal Co., Ltd. The thickness of each metal plate was 1.0 mm. Auxiliary materials like the vacuum bag and sealing tape were purchased from Airtech.

### 3.2 Microwave absorption measurement

The microwave absorption properties of prepared samples were measured by the free space method. Specifically, the sample was fixed at the front of a lens antenna (2.17~3.30 GHz, HENGDA MICROWAVE) connected to a vector network analyzer (VNA, N5244B, Keysight). Then, a microwave signal was generated by the VNA. The antenna focused the microwave beam on the sample and detected the reflected signal. In this way, the ratio of the reflected signal $S_{11} = 10\lg(R)$ in dB was recorded by the VNA, where $R$ is the reflectance in percentage. Note that no transmission existed in this experiment, since the thickness of each metal plate was much greater than the microwave penetration depth. Consequently, the absorbance (in percentage) could be calculated by $A=1-R$.

### 3.3 Microwave heating and welding experiments

After the measurement of microwave absorption, the samples were put into a self-developed octagonal microwave oven [31] for validating heating performance or conducting a welding experiment. The microwave oven was equipped with two solid-state sources and twelve magnetrons. The maximum output power of the two solid-state sources was 1000 W, with a working frequency of 915 MHz. As for the twelve magnetrons, their working frequency and the maximum output power were 2.45 GHz and 1500 W, respectively. The microwave energy was transmitted by waveguides, and radiated on the object being heated through slot antennas which were distributed on each side of the octagonal cavity. In the heating process, an infrared thermal imager (FLIR A310), located on the top surface of the cavity, was used to capture the in-plane temperature distribution of the sample. Simultaneously, the temperature at selected positions was monitored by some fiber-optic fluorescence sensors (Beijing DongFang RuiZe Technology Co., Ltd.) which could work from room temperature to 280 °C. In this way, desired temperature fields could be achieved by the closed-loop control of the power of microwave sources.

### 3.4 Characterization of materials

Mechanical tests were carried out to evaluate the quality of the welded plate using a universal testing machine (INSTRON 5982). Specifically, the welded interface was directly subjected to a tensile load, similar to the double cantilever beam test. The test speed was 1.0 mm/min, and the temperature was room temperature. Three kinds of specimens, with widths varying from 1 mm to 3 mm, were used in this experiment. For each one, at least three samples were tested. An optical microscope (BMM-50E, China ShangHai BiMu Instrument Co., Ltd.) was used to check the welded interface of the damaged specimens.

## 4 Results and discussions

### 4.1 Evaluation of microwave absorption

When the EMRs were designed, copper-clad polyimide films were etched with the required periodic planar structure by a laser printed circuit board etcher. Fig. 4(a) shows the periodically arranged EMRs in the case of an iron plate. After that, the EMRs backed by the dielectric spacer were introduced on the metal plate, and the microwave absorption properties of the MIM configuration were measured by the free space method.

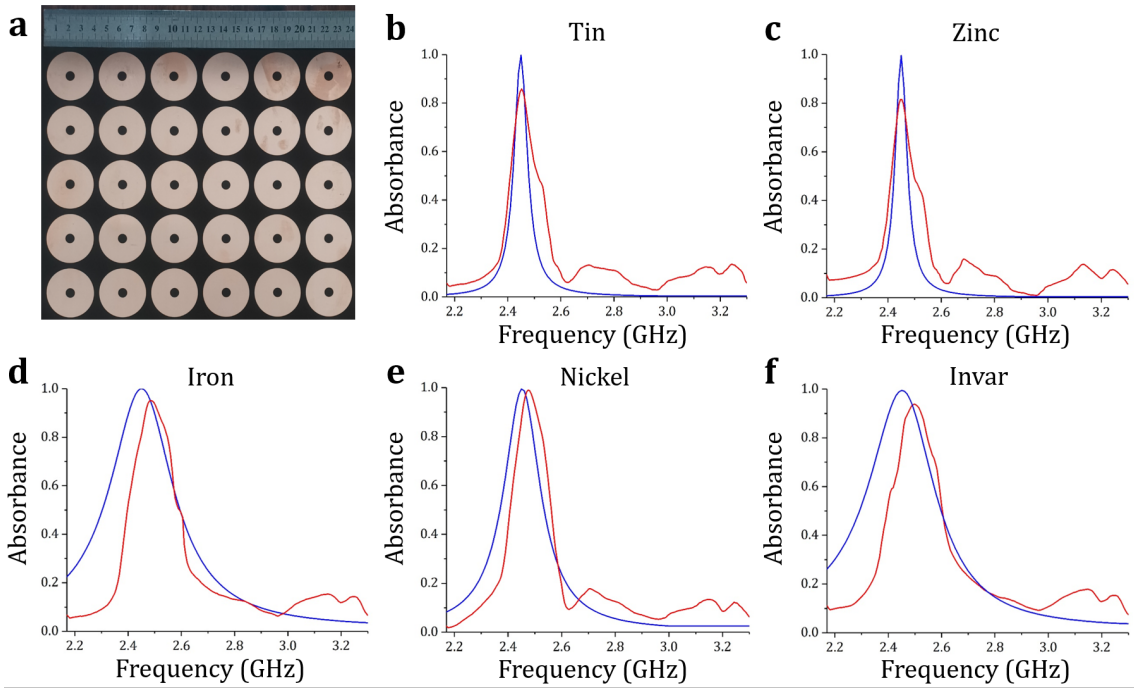


**Fig. 4.** (a) Photograph of the polyimide film-supported EMRs. (b-f) Simulated (blue curves) and measured (red curves) absorption spectra of 5 MIM configurations for a constant polarization angle at normal incidence.

The experimental results for a constant polarization angle at normal incidence are depicted in Fig. 4(b-f), as well as the simulated ones for comparison. For each configuration, an absorption peak with a center frequency around 2.45 GHz and a peak value close to 100% was also simulated. The experimental results agreed well with simulation results, while the maximum difference in the center frequency was only 0.05 GHz. It indicates that the proposed method makes solid metals completely microwave absorptive at room temperature, which is very interesting because solid metals are microwave reflective below their critical temperatures. Moreover, by comparing the absorption curves of the 5 MIM configurations it can be inferred that this method could apply to various metals, which lays a good foundation for potential industrial applications.

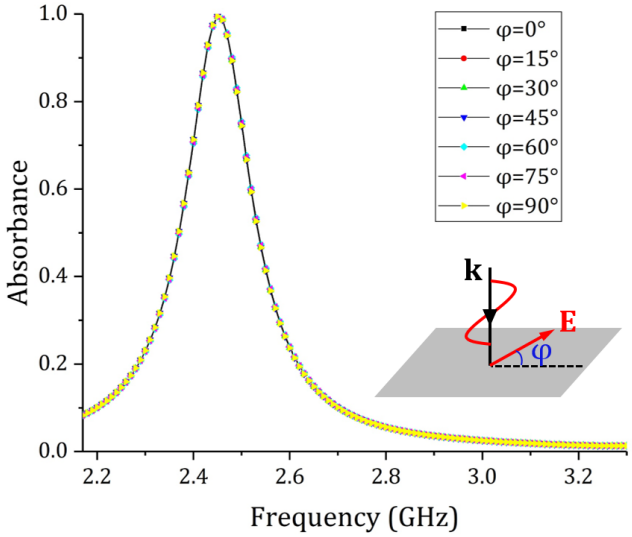


**Fig. 5.** Simulated absorption spectra of the MIM configuration (nickel plate) for different polarization angles ($\varphi$) at normal incidence.

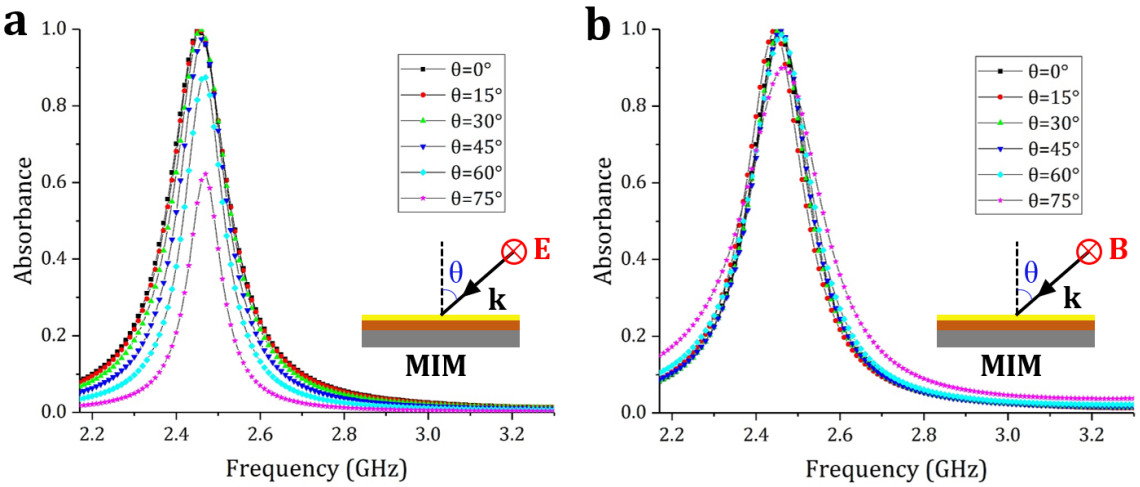


**Fig. 6.** Simulated absorption spectra of the MIM configuration (nickel plate) at different incident angles ($\theta$) for (a) TE polarized wave and TM polarized wave.

Considering that microwaves are incident on the material at various angles and the electric fields are also randomly oriented in all directions in the microwave cavity, the absorption of the MIM configuration under these conditions should be further studied. Taking the nickel plate as an example, Fig. 5 shows the simulated absorption spectra of the MIM configuration for different polarization angles ($\varphi$) at normal incidence. It can be seen that the absorption of the MIM configuration was insensitive to polarization angles, which was benefited from the geometric symmetry of the designed

EMRs. The absorption of the MIM configuration at different incident angles ($\theta$) for TE and TM polarized waves is presented in Fig. 6. For the TE mode, the performance was almost stable for the incident angle ranging from 0° to 45°, and the absorbance remained at ≥80% at 60° and ≥60% at 75°. For the TM mode, the absorption was almost independent of the incident angle. The absorbance was nearly 100% at 0° ~ 60° and reached 90% even at 75°. This phenomenon was mainly derived from the magnetic resonance between the MIM configuration and the incident microwave. Since the magnetic field of the TM polarized wave remained unchanged with the angle of incidence, it could efficiently drive the antiparallel currents at all incident angles [32]. As mentioned above, the idea can work over a wide range of incidence angles under both TE and TM polarized waves, and the absorption of the MIM configuration is insensitive to polarization angles. These advantages could be very beneficial for potential microwave heating applications.

**Table 2**

The power consumption of constituent elements in the MIM configurations of 5 materials.

| Materials | Power consumption (%) | | |
|---|---|---|---|
| | Copper units | Polyimide film | Solid metal |
| Tin | 19.6 | 36.2 | 44.2 |
| Zinc | 23.0 | 41.4 | 35.6 |
| Iron | 0.8 | 4.9 | 94.3 |
| Nickel | 2.5 | 10.1 | 87.4 |
| Invar | 1.1 | 5.2 | 93.7 |

After demonstrating the excellent microwave absorption of the MIM configuration, the power consumption of its constituent elements was investigated by time-dependent simulation using the software package CST Microwave Studio [31]. The results are summarized in Table 2. It can be

observed that most of the energy was consumed in the solid metals of magnetic materials (iron, nickel and invar). However, the consumption of the dielectric spacer became considerable for non-magnetic metals (tin and zinc), which might be improved using new lossless dielectric materials to replace polyimide films. In any case, the power consumption of the EMRs was the smallest because of the high conductivity of copper.

### 4.2 Microwave heating of metal plates

Microwave heating experiments were carried out on metal plates (300×300×1.0 $mm^3$) of the 5 materials listed in Table 2. For the nickel plate, a relatively rapid microwave heating was achieved under the available maximum power intensity of 2.83 $mW/cm^3$. Fig. 7(a) shows the temperature profile measured by the fiber-optic thermo-sensor, as well as the in-plane temperature distribution captured by the infrared thermal imager. It can be seen that the nickel plate heated up immediately once the MW radiation was switched on. Remarkably, the heating rate on the top surface exceeded 500 °C/min in the initial stage, which could be further improved by employing a higher power density. As the temperature increased, the heat dissipation from the plates to the surrounding environment (maintained at room temperature) increased as well, while the ramp rate decreased a little. When the temperature reached about 220 °C, the microwave power was turned off, and the plates cooled down naturally. During this process, the pattern of EMRs was clearly observed, which demonstrated the effect of the designed EMRs very well. In addition to the rectangular sheet, experiments on irregularly shaped plates were also carried out. Fig. 7(b) and (c) present the infrared thermal images of a trapezoid and quadrant nickel plates during the microwave heating process. It can be seen that, compared with resistance heating, the proposed method has outstanding advantages in heating irregularly shaped parts of inconstant cross-sections.

Microwave heating experiments, with a lower power intensity, were also carried out on metal plates (300×300×1.0 $mm^3$) of 5 materials to verify the applicability of the proposed method. Table 3 summarizes the heating rates on the surfaces of the 5 materials measured by fiber-optic thermo-sensors.

It can be seen that the heating performance of all 5 materials were very similar under the constant power density, which might be derived from their similar microwave absorption as shown in Fig. 4. As mentioned above, the developed technology was able to convert nearly 100% of microwave energy to heat solid metals. These results are quite exciting because solid metals are totally reflective below their critical temperatures, and metallic objects are often prohibited in microwave ovens.

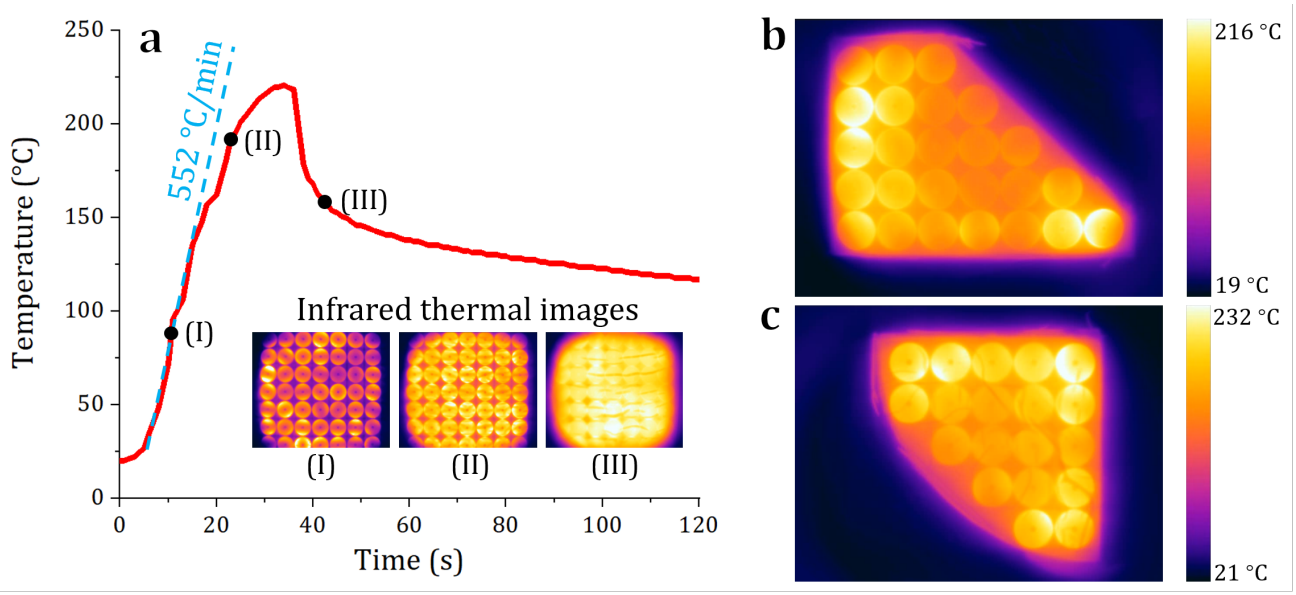


**Fig. 7.** (a) A rapid microwave heating process on a rectangular nickel plate. Infrared thermal images of (b) trapezoid and (c) quadrant nickel plates during the microwave heating process.

**Table 3**

The heating rates on the surfaces of metal plates of 5 materials.

| Materials | Tin | Zinc | Iron | Nickel | Invar |
|---|---|---|---|---|---|
| Heating rates (°C/min) | 76.9 | 64.4 | 82.2 | 76.9 | 78.6 |

To investigate the temperature distribution along the thickness direction, six nickel plates were stacked together, with polyimide film-supported EMRs applied to the surface of the top one. Fiber-optic fluorescence sensors were used to monitor the temperature at selected positions. Fig. 8 shows the temperature profiles in the thickness direction (measured from the 6 stacked plates and shown by

colored curves) and the air inside the oven, where a temperature gradient is clearly visible. It is because that the depth of penetration into solid metals was very small (in microns), the plate below was mainly heated by conduction of the plate above, and the heating rate was high. Although this problem may be improved by applying EMRs on more surfaces of solid metals, the advantage of the proposed method may not be obvious when heating metal plates of large thickness.

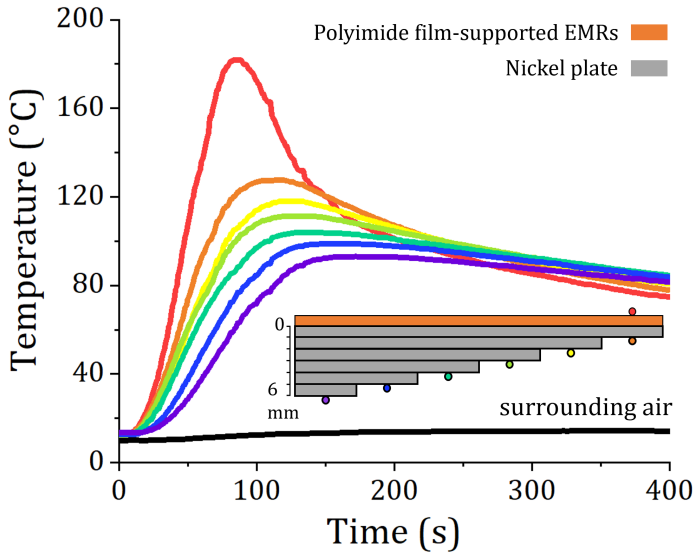


**Fig. 8.** Temperature profiles of stacked nickel plates during the microwave heating process.

In order to investigate the durability of the EMRs, a thermal cycling test was carried out, and the variation of the microwave absorption properties of the MIM configuration was evaluated. A total of 10 heating-cooling cycles were adopted, as shown in the inset of Fig. 9. The microwave absorption spectra of the MIM configuration after 0 (blue), 1 (yellow), 2 (red), 3 (green) and 10 (purple) heating-cooling cycles are presented in Fig. 9. It was found that the center frequency of the absorption peak of the MIM configuration shifted from 2.45 GHz to 2.54 GHz after one heating-cooling process, and then it remained unchanged. Fortunately, a certain absorbance (≥35%) was always maintained at 2.45 GHz, so the MIM configuration presented a good microwave heating capability during the 10 repeated processes. Through univariate analysis, it was found that the variation in the microwave absorption was caused by the adopted dielectric spacer. It can be seen that, when the dielectric spacer was replaced with polyimide films that were not heated, the absorption properties of the MIM configuration returned

to the original state (see the dashed purple line in Fig. 9). This means that the EMRs can be used repeatedly by choosing more suitable materials as the dielectric spacer in the future.

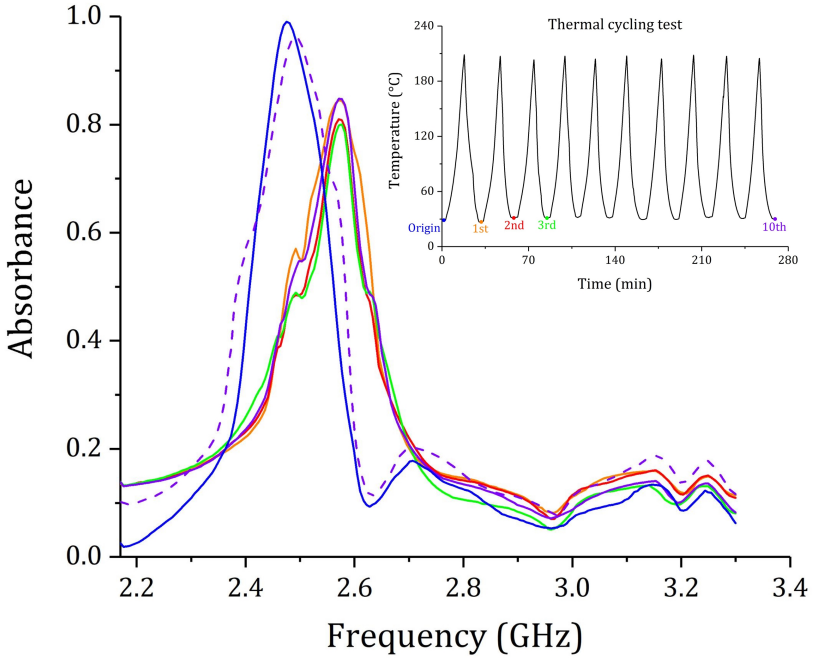


**Fig. 9.** Measured absorption spectra of the MIM configuration (nickel plate) after 0 (blue), 1 (yellow), 2 (red), 3 (green), and 10 (purple) heating-cooling cycles, with an inset showing the temperature curves recorded during the thermal cycling test.

### 4.3 Patterned microwave heating of metal plates

As stated earlier, the microwave heating performance was directly dependent on the EMRs introduced on the metal plates being heated. Thus, any required heating patterns could be realized readily by arranging the EMRs correspondingly. For example, EMRs were arranged into four English letters on a nickel plate (200×200×1.0 $mm^3$) to form the word "IDEA" (Fig. 10). When the microwave source was activated, ‘IDEA’ was illuminated under the thermal imager. This could enable a plethora of applications like localized heating, thermal display, and so on.

In addition to arranging EMRs, the patterned microwave heating effect can be further enhanced by taking the advantage of EMR design. The absorbance of the MIM configuration can be easily adjusted by changing the inner diameter of the copper rings. As shown in Fig. 11, absorbance changed from 99% to 38% in different locations of EMRs. Accordingly, a patterned heating performance with

varying temperatures could be achieved. The heating effect of the EMR changes could be predicted by combining the electromagnetic model used in this experiment with the existing heat transfer model, which will be carried out in the authors' future work.

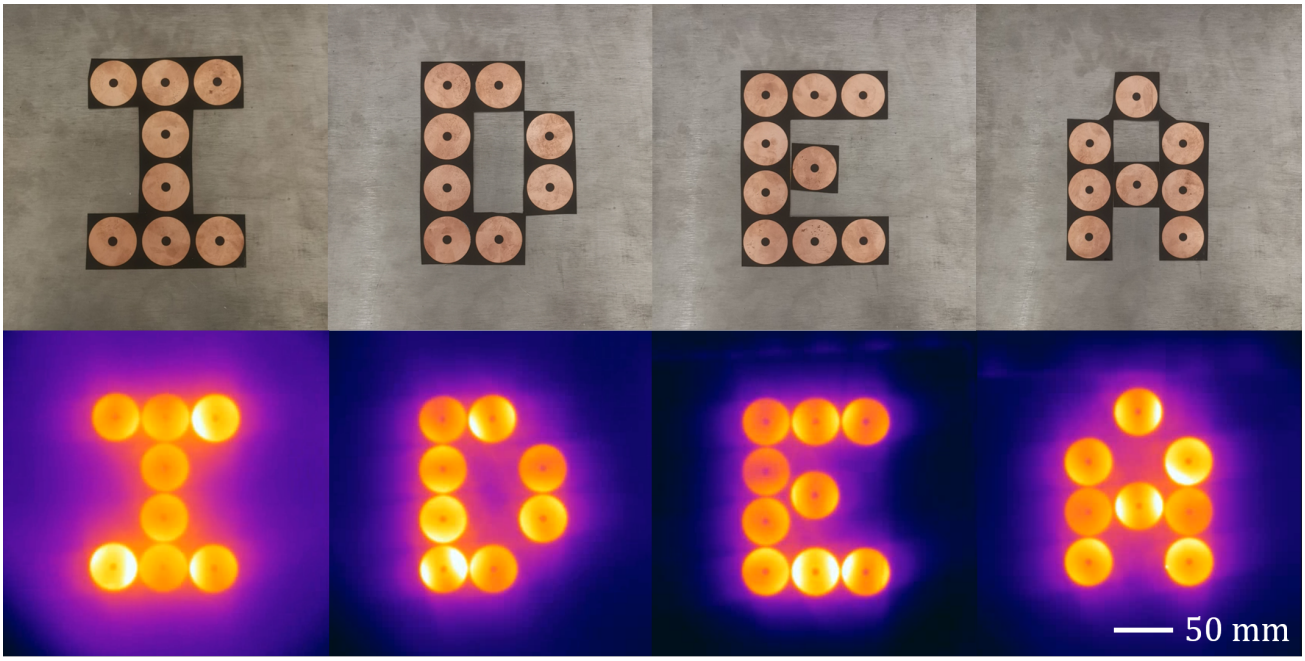


**Fig. 10.** Microwave heating by properly arranging EMRs in patterns.

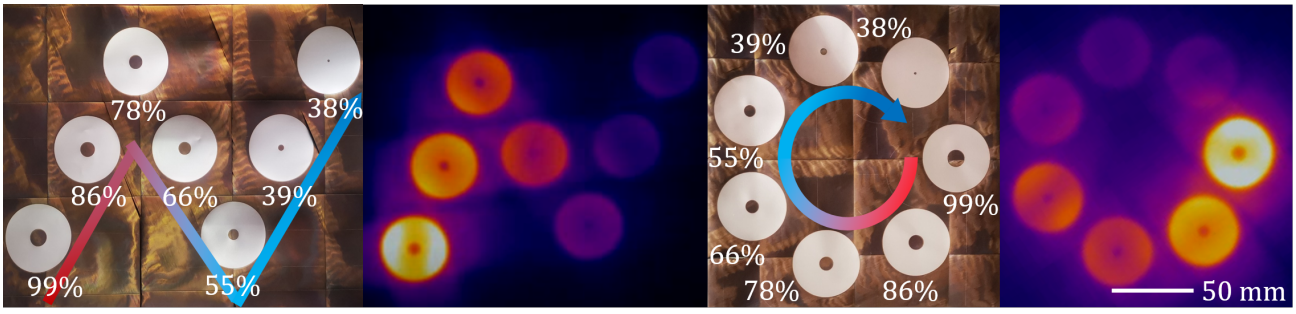


**Fig. 11.** Patterned microwave heating with varying temperatures.

Furthermore, the heating pattern could be dynamically controlled during the heating process by adding the freedom of frequency. This is because MIM configurations were narrowband absorbers (Fig. 4), and their resonant frequency was determined by the parameters of EMRs. Therefore, if the MIM configuration is designed to be sensitive to different frequencies in different areas, a dynamically patterned heating effect can be achieved by applying microwave radiations of these frequencies. For instance, two different EMRs working at 915 MHz and 2.45 GHz were developed and applied on the

nickel plate, as shown in Fig. 12(a). When the microwave source of 915 MHz was turned on, the corresponding areas were quickly heated, resulting in a big ring as shown in Fig. 12(b). After that, the radiation of 2.45 GHz was activated as well. As a result, the surrounding small rings became visible as shown in Fig. 12(c). Then the microwave source of 915 MHz was turned off, and only the surrounding rings remained as shown in Fig. 12(d).

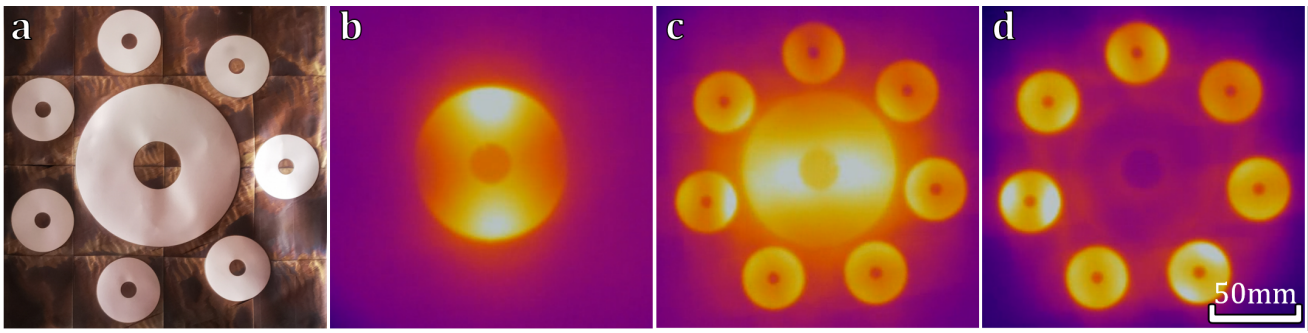


**Fig. 12.** Dynamically patterned heating with different frequencies applied: (a) photograph of adopted EMRs; thermal images under (b) 915 MHz, (c) 915 MHz and 2.45 GHz and (d) 2.45 GHz.

### 4.4 Multi-zone microwave welding of metal plates

Since on-demand temperature distribution can be achieved by adjusting the EMRs, a multi-zone microwave processing paradigm can be developed accordingly. In this experiment, it was only tested for a welding process. Limited by the maximum power of the available microwave source, the welding experiment was carried out on tin plates which have a melting temperature of about 230 °C. As shown in Fig. 13(a), to weld two smaller tin plates (200×85×1.0 $mm^3$) to a bigger one (200×200×1.0 $mm^3$), four EMRs were used to realize local microwave heating at four different wielding positions simultaneously. The welded plate is exhibited in Fig. 13(b). As shown, the shape and size of the welded region were almost the same as that of the EMR. Note that both the shape and size of the EMRs could be designed to meet different application scenarios.

Mechanical tests were carried out to evaluate the quality of the welded plate. Specifically, several specimens (with widths varying from 1 mm to 3 mm) were cut from the welded tin plate and placed on a universal testing machine. During the test, the welded interface was directly subjected to the

tensile load which was applied at a speed of 1.0 mm/min, similar to the double cantilever beam test. Fig. 13(c) depicts the load-displacement curves of these specimens, where an intrinsically ductile characteristic of tin was presented. It can be noted that fracture failure rather than de-bonding of welded interface occurred during the test process of all specimens. As a consequence, the wider the specimen, the higher the peak load.

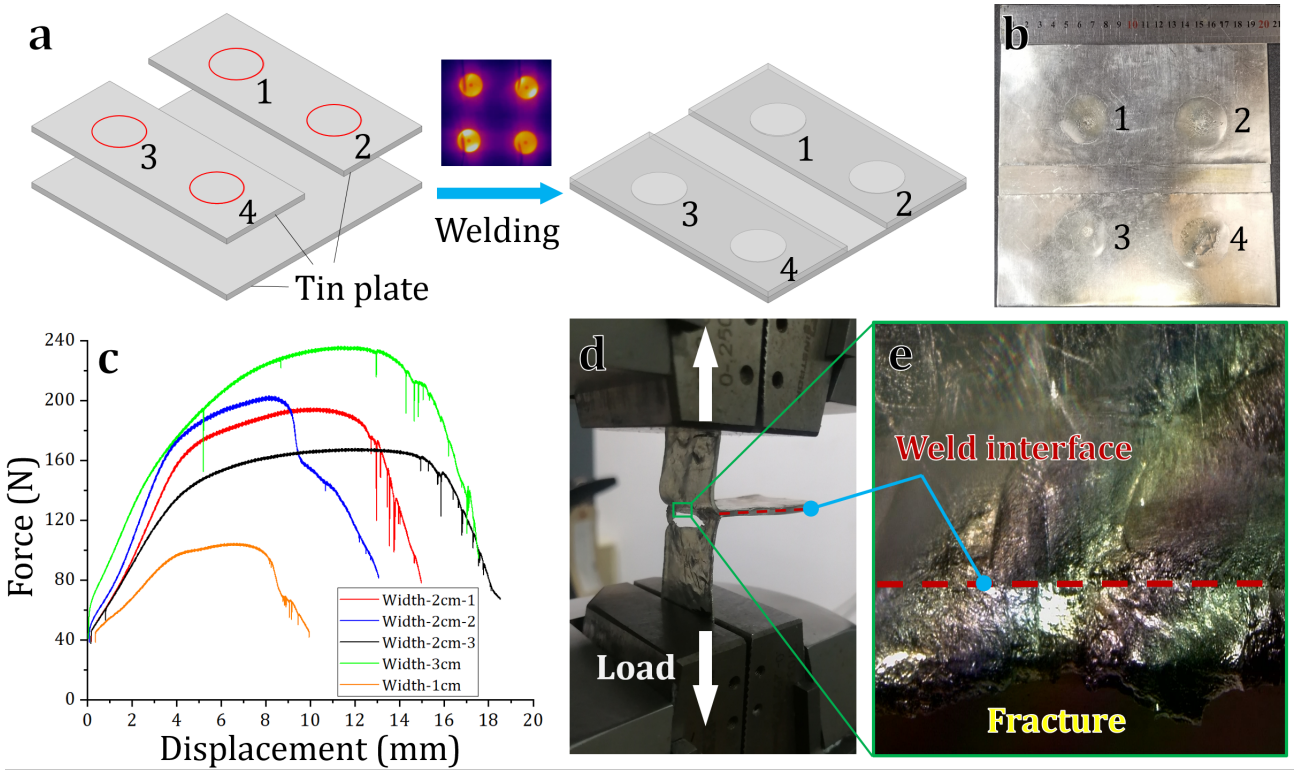


**Fig. 13.** Multi-zone microwave welding of tin plates: (a) illustration of the welding process; (b) photograph of the welded tin plate; (c) load-displacement curves of specimens with varying widths; (d) photograph of the fracture failure mode; (f) optical microscopy of the welded interface.

Taking the specimen with a width of 2 mm as an example, the representative fracture failure mode is presented in Fig. 13(d). The welded interface of the damaged specimen was further checked using an optical microscope. The corresponding result is presented in Fig. 13(e). As no de-bonding of the welded interface could be found, the quality of the welded plate was proved. As mentioned above, for the first time, a proof-of-principle for microwave heating and processing of solid metals has been realized in the experiment.

## 5 Conclusions and further work

The experimental results proved the proposed theory and hypothesis of a new method that makes solid metals completely microwave absorptive by adopting electromagnetic resonators (EMRs), particularly because those materials are essentially reflective to microwave below certain critical temperatures. In this research, microwave heating of metal plates of 5 materials including magnetic (iron, nickel, and invar) and non-magnetic (tin and zinc) were used for testing. A patterned microwave heating process was demonstrated by adjusting EMRs and microwave radiations. A new multi-zone microwave processing paradigm was developed and tested for a welding process. Compared with existing heating technologies, the new microwave heating method provides a potential solution for efficient heating of complex shaped metal parts for manufacturing processes such as forming, welding, and heat treatment. It is promising that more efficient microwave heating effects can be achieved in the future, and a series of microwave processing technologies would be developed by the authors, using microwave equipment with a higher power density and by adopting materials with higher temperature resistance for EMRs.

## 6 Funding

This project was funded by the National Natural Science Foundation of China (Grant no. 52105364, 51875288, and 52090052), and supported by the XPLORER PRIZE.

## 7 Author contributions

Jing Zhou: Conceptualization, Methodology, Investigation, Writing. Yingguang Li: Conceptualization, Supervision, Project Management. Tao Yang: Investigation, Validation, Visualization, Writing. Wenzheng Xue: Investigation, Validation, Visualization, Writing. Xiaozhong Hao: Supervision, Design of Experiment. James Gao: Supervision, Research Methodology, Writing.

## 8 Conflict of interest

The authors declare that they have no conflict of interest.

**References**

[1] Yang DY, Bambach M, Cao J, Duflou JR, Groche P, Kuboki T, Sterzing A, Tekkaya AE, Lee C W (2018) Flexibility in metal forming. CIRP Ann-Manuf Techn 67:743–765. https://doi.org/10.1016/j.cirp.2018.05.004

[2] Zhang P, Zhu L, Luo S, Luo J (2019) Hot stamping forming and finite element simulation of USIBOR1500 high-strength steel. Int J Adv Manuf Tech 103:3187-3197. https://doi.org/10.1007/s00170-019-03727-w

[3] Marques MJ, Ramasamy A, Batista AC, Nobre JP, Loureiro A (2015) Effect of heat treatment on microstructure and residual stress fields of a weld multilayer austenitic steel clad. J Mater Process Tech 222:52-60. https://doi.org/10.1016/j.jmatprotec.2015.03.004

[4] Chen K, Zhan L, Xu Y, Ma B, Zeng Q, Luo S (2022) Optimizing strength and ductility in 7150 Al alloys via rapid electropulsing cyclic heat treatment. J Alloy Compd 903:163985. https://doi.org/10.1016/j.jallcom.2022.163985

[5] Oliveira JP, Miranda RM, Fernandes FMB (2017) Welding and joining of NiTi shape memory alloys: a review. Prog Mater Sci 88:412-466. https://doi.org/10.1016/j.pmatsci.2017.04.008

[6] Lee Y, Cheon J, Kang M (2021) Vacuum laser beam welding characteristics for aluminum alloys and its effects on plasma plume generation and laser weldability. Int J Adv Manuf Tech 115:531-539. https://doi.org/10.1007/s00170-021-07081-8

[7] Chen W, Zhu Y, Chen L, Chen F, Liu B (2021) Effects of different process parameters on mechanical properties and microstructures of hot stamping boron steel. Int J Adv Manuf Tech 114:939-948. https://doi.org/10.1007/s00170-021-06736-w

[8] Tekkaya AE, Allwood JM, Bariani PF, Bruschi S, Cao J, Gramlich S, Groche P, Hirt G, Ishikawa T, Löbbe C, Lueg-Althoff J, Merklein M, Misiolek WZ, Pietrzyk M, Shivpuri R, Yanagimoto J

(2015) Metal forming beyond shaping: Predicting and setting product properties. CIRP Ann-Manuf Techn 64:629–653. https://doi.org/10.1016/j.cirp.2015.05.001

[9] Halford B (2015) Zone control of tool temperature. US 9,034,234 B2.

[10] Jhajj KS, Slezak SR, Daun KJ (2015) Inferring the specific heat of an ultra high strength steel during the heating stage of hot forming die quenching, through inverse analysis. Appl Therm Eng 83:98-107. https://doi.org/10.1016/j.applthermaleng.2015.03.013

[11] Landgrebe D, Putz M, Schieck F, Sterzing A, Rennau A (2015) Towards efficient, interconnected and flexible value chains - examples and innovations from research on production technologies. In: Proceedings of 5th International Conference on Accuracy in Forming Technology. Chemnitz, Germany, pp 61-78.

[12] Duflou JR, Callebaut B, Verbert J, De Baerdemaeker H (2007) Laser assisted incremental formi ng: formability and accuracy improvement. CIRP Ann-Manuf Techn 56(1):273-276. https://doi.org /10.1016/j.cirp.2007.05.063

[13] Lee EH, Hwang JS, Lee CW, Yang DY, Yang WH (2014) A local heating method by near-infrar ed rays for forming of non-quenchable advanced high-strength steels. J Mater Process Tech 214(4): 784–793. https://doi.org/10.1016/j.jmatprotec.2013.11.023

[14] Biesuz M, Saunders T, Ke D, Reece MJ, Hu C, Grasso S (2021) A review of electromagnetic pr ocessing of materials (EPM): Heating, sintering, joining and forming. J Mater Sci Technol 69:239-272. https://doi.org/10.1016/j.jmst.2020.06.049

[15] Mori K, Maki S, Tanaka Y (2005) Warm and hot stamping of ultra high tensile strength steel she ets using resistance heating. CIRP Ann-Manuf Techn 54(1):209-212. https://doi.org/10.1016/S0007 -8506(07)60085-7

[16] Mori K, Bariani PF, Behrens BA, Brosius A, Bruschi S, Maeno T, Merklein M, Yanagimoto J (2 017) Hot stamping of ultra-high strength steel parts. CIRP Ann-Manuf Techn 66(2):755–777. https ://doi.org/10.1016/j.cirp.2017.05.007

[17] Kolleck R, Veit R, Merklein M, Lechler J, Geiger M (2009) Investigation on induction heating f or hot stamping of boron alloyed steels. CIRP Ann-Manuf Techn 58(1):275–278. https://doi.org/10 .1016/j.cirp.2009.03.090

[18] Li H, Zhao Z, Xiouras C, Stefanidis GD, Li X, Gao X (2019) Fundamentals and applications of microwave heating to chemicals separation processes. Renew Sust Energ Rev 114:109316. https://d oi.org/10.1016/j.rser.2019.109316

[19] Li Y, Cheng L, Zhou J (2018) Curing multidirectional carbon fiber reinforced polymer composit es with indirect microwave heating. Int J Adv Manuf Tech 97:1137-1147. https://doi.org/10.1007/s 00170-018-1974-1

[20] Mishra RR, Sharma AK (2016) Microwave-material interaction phenomena: Heating mechanism s, challenges and opportunities in material processing. Compos Part A-Appl S 81:78-97. https://doi .org/10.1016/j.compositesa.2015.10.035

[21] Guan C, Zhan L, Liu G, Yang X, Dai G, Jiang C, Chen X (2020) Optimization of a high-pressure microwave curing process for T800/X850 carbon fiber-reinforced plastic. High Perform Polym 32(1): 30-38. https://doi.org/10.1177/0954008319846923

[22] Yin Z, Hao Z, Peng H, Yuan J (2022) A new β-SiAlON ceramic tool prepared by microwave sintering and its cutting performance in high-speed dry machining Inconel718. Int J Adv Manuf Tech 118:3105-3117. https://doi.org/10.1007/s00170-021-08170-4

[23] Zhou J, Li Y, Li N, Liu S, Cheng L, Sui S, Gao J (2018) A multi-pattern compensation method to ensure even temperature in composite materials during microwave curing process. Compos Part A-Appl S 107:10-20. https://doi.org/10.1016/j.compositesa.2017.12.017

[24] Zhou J, Li Y, Li D, Wen Y (2019) Online learning based intelligent temperature control during p olymer composites microwave curing process. Chem Eng J 370:455-465. https://doi.org/10.1016/j. cej.2019.03.204

[25] Zhou J, Li Y, Zhu Z, Xu E, Li S, Sui S (2022) Microwave heating and curing of metal-like CFRP laminates through ultrathin and flexible resonance structures. Compos Sci Technol 218:109200. https://doi.org/10.1016/j.compscitech.2021.109200

[26] Lingappa SM, Srinath MS, Amarendra HJ (2017) An experimental investigation to find the critical (coupling) temperature in microwave hybrid heating of bulk metallic materials. Mater Res Express 4:106521. https://doi.org/10.1088/2053-1591/aa931e

[27] Roy R, Agarwal D, Chen J, Gedevanishvili S (1999) Full sintering of powdered-metal bodies in a microwave field. Nature 399:668-670. https://doi.org/10.1038/21390

[28] Zhang Y, Agrawal DK, Cheng J, Slawecki T (2018) Microwave power absorption mechanism of metallic powders. IEEE T Microw Theory 66(5):2107-2115. https://doi.org/10.1109/TMTT.2018.2804980

[29] Sun S, He Q, Hao J, Xiao S, Zhou L (2019) Electromagnetic metasurfaces: physics and applications. Adv Opt Photonics 11(2):380-479. https://doi.org/10.1364/AOP.11.000380

[30] Zhou J, Economon EN, Koschny T, Soukoulis MS (2006) Unifying approach to left-handed material design. Opt let 31(24):3620-3622. https://doi.org/10.1364/OL.31.003620

[31] Zhou J, Li Y, Liu S, Zhang Y, Wang P, Sui S (2022) Zone-regulated microwave heating of CFRP laminates via ultrathin and flexible resonance structures with different working frequencies. Compos Commun 29:101016. https://doi.org/10.1016/j.coco.2021.101016

[32] Liu N, Mesch M, Weiss T, Hentschel M, Giessen H (2010) Infrared perfect absorber and its application as plasmonic sensor. Nano Lett 10(7):2342-2348. https://doi.org/10.1021/nl9041033

**Figure captions**

**Fig. 1.** The normally incident microwave signal (a) and the response of the EMRs and solid metal (b-c), where **E**, **H**, and **k** denote the direction of the electric field, magnetic field, and wave propagation respectively.

**Fig. 2.** The MIM configuration and its constituent elements.

**Fig. 3.** (a) The normally incident microwave signal (1 W). (b-c) The simulated current distribution on the EMR-covered iron surface.

**Fig. 4.** (a) Photograph of the polyimide film-supported EMRs. (b-f) Simulated (blue curve) and measured (red curve) absorption spectra of 5 MIM configurations for a constant polarization angle at normal incidence.

**Fig. 5.** Simulated absorption spectra of the MIM configuration (nickel plate) for different polarization angles ($\varphi$) at normal incidence.

**Fig. 6.** Simulated absorption spectra of the MIM configuration (nickel plate) at different incident angles ($\theta$) for (a) TE polarized wave and TM polarized wave.

**Fig. 7.** (a) A rapid microwave heating process on a rectangular nickel plate. Infrared thermal images of (b) trapezoid and (c) quadrant nickel plates during the microwave heating process.

**Fig. 8.** Temperature profiles of stacked nickel plates during the microwave heating process.

**Fig. 9.** Measured absorption spectra of the MIM configuration (nickel plate) after 0 (blue), 1 (yellow), 2 (red), 3 (green), and 10 (purple) heating-cooling cycles, with an inset showing the temperature curves recorded during the thermal cycling test.

**Fig. 10.** Microwave heating by properly arranging EMRs in patterns.

**Fig. 11.** Patterned microwave heating with varying temperatures.

**Fig. 12.** Dynamically patterned heating with different frequencies applied: (a) photograph of adopted EMRs; thermal images under (b) 915 MHz, (c) 915 MHz, and 2.45 GHz, as well as (d) 2.45 GHz.

**Fig. 13.** Multi-zone microwave welding of tin plates: (a) illustration of the welding process; (b) photograph of the welded tin plate; (c) load-displacement curves of specimens with varying widths; (d) photograph of the fracture failure mode; (f) optical microscopy of the welded interface.